THE STABILITY OF HIGH SPEED AXIALLY MOVING MATERIALS

N. C. Perkins†
S.-J. Hwang ‡
Mechanical Engineering and Applied Mechanics
2250 G. G. Brown Laboratories
University of Michigan
Ann Arbor, MI 48109-2125

Abstract

This paper focuses on the stability of axially moving beam-like materials (e.g., belts, bands, paper and webs) which translate at speeds near to and above the so-called "critical speed stability limit." A theoretical model for an axially moving beam is presented which accounts for geometrically nonlinear beam deflections and the initial beam curvature generated by supporting wheels and pulleys. Analysis of steady response reveals that the beam possesses multiple, non-trivial equilibrium states when translating at super-critical speeds. The equations of motion are linearized about these equilibria and their stability is determined from the eigensolutions of a discretized model. This analysis leads to new conclusions regarding the stability of axially moving materials. In particular, it is shown that the critical speed behavior commonly associated with axially moving material problems represents an idealized phenomenon which does not exist when imperfections, such as initial curvature, are present.

1. Introduction

Axially moving material problems consider the dynamic response, vibration and stability of long, slender members which are in a state of uniform translation. Examples of systems employing axially moving materials include magnetic tape recording devices, belt and chain drives, thread and fiber winders, band saws, paper and web handling machinery, and cable pay-out/reel-in systems. Principal developments in the literature on axially moving materials are reviewed by Mote[1] and, more recently, by Wickert and Mote[2].

Traditional models of axially moving materials[1] represent the translating element as either a taut string or an Euler-Bernoulli beam that is drawn perfectly straight under large tension. The analysis of such geometrically *perfect* systems leads to the prediction that the stability of axially moving materials is limited to translation speeds below a theoretical *critical speed*. At the critical speed, the translating element experiences a divergence-type instability.

†Assistant Professor, Member AIAA, Associate Member ASME.
‡Research Assistant.

Recently however, studies have demonstrated that critical speed behavior for a class of axially moving materials is an idealized phenomenon that does not occur when *imperfections* are correctly accounted for in the model. Perkins and Mote[3] found that initial sag due to gravity creates a stabilizing speed-tensioning effect that permits the sagged equilibrium to remain stable at very high translation speeds. In addition, the initial sag creates the possibility of a second arch-like equilibrium which becomes stabilized at high translation speeds[4]. These studies[3,4] focus on flexible axially moving materials (e.g., threads, fibers, chains and cables) and they do not consider the flexural rigidity important in the modeling of translating beam-like elements (e.g., bands, belts, paper and webs). Since the stability of a translating beam is essentially a buckling problem[5], it is also potentially very sensitive to imperfections.

This paper investigates the stability of beam-like elements at translation speeds which exceed the classical "critical speed stability limit". A model for an axially moving beam is presented which accounts for imperfections described by initial beam curvature and geometrically nonlinear beam deflections. The equations of equilibrium are examined first and the possible equilibrium states of the translating beam are described. The equations of motion are then linearized about these equilibria and stability is assessed through the eigensolutions of a discretized model.

2. Theoretical Model

A theoretical model is presented which governs the planar motion of a translating beam with initial curvature. Figure 1 defines the problem of interest and shows a translating beam which is initially held in equilibrium under tension N and moments M applied at two supports. The bending moments result from the curvature of the supporting wheels or pulleys (not shown) and the tension derives from an externally applied pre-load. Support flexibility is included in the model by allowing the left support to be elastically restrained in translation by a spring of stiffness K. The curve χ^i denotes the equilibrium configu-

ration of the beam centerline which has length L between the supports and lies in X-Y plane. The planar motion the beam centerline about its equilibrium configuration is described by $\mathbf{U}(S,T)$ where S denotes the arc length coordinate measured along χ^i and T denotes time. This motion, $\mathbf{U}(S,T) = U_1\mathbf{e}_1^i + U_2\mathbf{e}_2^i$ describes the final configuration χ^f and is resolved into components aligned with the local tangential, $\mathbf{e}_1^i$, and normal, $\mathbf{e}_2^i$, directions defined by χ^i. In Figure 1, C represents the beam particle translation speed relative to χ^i and χ^f.

Hamilton's principle is used to derive the equations of motion which are based on the following assumptions.

1. The beam is a homogeneous, one-dimensional elastic continuum obeying a linear stress-strain relationship.
2. Extensions of the beam are described by the Lagrangian strain of the centerline.
3. The motion of the beam is restricted to the X-Y plane.
4. The beam may undergo large static deflections, and additional deflections from the curved equilibrium are described using a nonlinear extension of Love rod theory[6].
5. Rotary inertia due to bending and strain energy due to shear may be neglected assuming the beam cross-sectional dimensions are small compared to its length.
6. Gravitational and dissipative forces may be neglected.
7. The beam mass flux is constant.

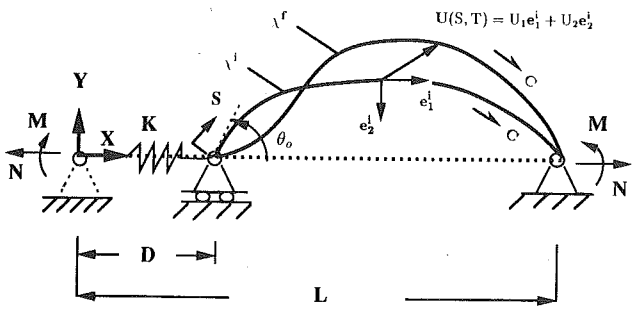

Figure 1: Definition diagram for curved, axially moving beam. Beam centerline is shown in three states: 1) unbuckled configuration (dotted line), 2) buckled equilibrium configuration χ^i, and 3) final configuration χ^f.

With these assumptions, expressions for the beam strain energy, kinetic energy and work are derived for use in Hamilton's principle.

The strain energy of the beam is composed of terms associated with the extension of the centerline and the flexure about the binormal (out-of-plane) axis. The Lagrangian strain of the centerline ϵ^f in its final configuration is related to the displacements U_1 and U_2 and the curvature $\mathcal{K}^i$ of the centerline in its initial configuration χ^i through[3],

$$\epsilon^f = \epsilon^i + \triangle\epsilon, \tag{1}$$

where

$$\triangle\epsilon = U_{1,s} - \mathcal{K}^i U_2 + \frac{1}{2}[(U_{2,s} + \mathcal{K}^i U_1)^2 + (U_{1,s} - \mathcal{K}^i U_2)^2], \tag{2}$$

and ϵ^i is the Lagrangian strain of the beam centerline in χ^i. In a similar fashion, the final curvature of the beam centerline $\mathcal{K}^f$ is related to the initial curvature $\mathcal{K}^i$ and the displacements U_1 and U_2 through

$$\mathcal{K}^f = \mathcal{K}^i + \triangle\mathcal{K}, \tag{3}$$

where

$$\triangle\mathcal{K} = a_{2,s} + (a_1 - 1)a_{2,s}, \tag{4}$$

$$a_1 = 1 + U_{1,s} - \mathcal{K}^i U_2, \tag{5}$$

$$a_2 = U_{2,s} + \mathcal{K}^i U_1. \tag{6}$$

The expression for $\triangle\mathcal{K}$ is derived from a nonlinear extension of Love rod theory[6]. Using (1) and (3), the strain energy of the beam in the final configuration is

$$\pi_s^f = \pi_s^i + \int_o^L [P^i \triangle\epsilon + EI\mathcal{K}^i \triangle\mathcal{K}]dS + \frac{1}{2}\int_o^L [EA(\triangle\epsilon)^2 + EI(\triangle\mathcal{K})^2]dS, \tag{7}$$

where π_s^i is the strain energy of the curved beam in χ^i, $P^i(S) = EA\epsilon^i(S)$ is the beam tension in χ^i, E is Young's modulus, I is the principal area moment about the binormal axis and A is the beam cross-sectional area.

The kinetic energy of the curved beam in χ^f is given by

$$\pi_k^f = \frac{1}{2}\int_o^L (\mathbf{V}^f * \mathbf{V}^f)\rho A dS, \tag{8}$$

where the velocity,

$$\mathbf{V}^f = \mathbf{U}_{,T} + C\mathbf{U}_{,S} + C\mathbf{e}_1^f, \tag{9}$$

represents the absolute velocity of a beam particle and ρ is the beam density.

The total work done by the bending moments M, the tension force N and the spring is

$$\pi_w = -M(a_2 + \theta_o)\,|_0^L - N[U_1(0,T)cos\theta_o - U_2(0,T)sin\theta_o + D] + \frac{1}{2}K[U_1(0,T)cos\theta_o - U_2(0,T)sin\theta_o + D]^2, \tag{10}$$

where $\theta(S)$ is the angle of inclination of the beam centerline in χ^i, $\theta_o = \theta(0)$, and D is the horizontal distance the left support moves during the static deformation leading to χ^i. $\theta(s)$ and D are related through

$$D = L - \int_0^L cos\theta(S)dS. \tag{11}$$

Following Benjamin[7], the correct statement of Hamilton's principle for this system with mass transport is

$$\delta[\int_{T_1}^{T_2} (\pi_k^f - \pi_s^f + \pi_w)dT] - \int_{T_1}^{T_2} \rho AC[\frac{d}{dT}(\mathbf{R}^i + \mathbf{U}) + C\mathbf{e}_1^f] * \delta\mathbf{U}\,|_0^L\, dT = 0. \tag{12}$$

Substituting (1)-(11) into (12) and taking the first variation leads to the following nonlinear equations governing planar motion:

tangential component, U_1

$$[(P^i + EA\triangle\epsilon)a_1]_{,s} - [(P^i + EA\triangle\epsilon)\mathcal{K}^i a_2] - EI\mathcal{K}^f\mathcal{K}^i_{,s}a_1 + EI[\mathcal{K}^f(a_{2,s} + \mathcal{K}^i a_1)]_{,s} = \rho A\{(U_{1,T} + Ca_1)_{,T} + C(U_{1,T} + Ca_1)_{,s} - C\mathcal{K}^i(U_{2,T} + Ca_2)\}, \quad (13)$$

normal component, U_2

$$[(P^i + EA\triangle\epsilon)a_2]_{,s} + \mathcal{K}^i a_1[P^i + EA\triangle\epsilon] + EI\mathcal{K}^f\mathcal{K}^i a_{2,s} - EI[\mathcal{K}^f a_1]_{,ss} = \rho A\{(U_{2,T} + Ca_2)_{,T} + C(U_{2,T} + Ca_2)_{,s} + C\mathcal{K}^i(U_{1,T} + Ca_1)\}, \quad (14)$$

with the boundary conditions:

$$U_1(L,T) = U_2(L,T) = 0, \quad (15)$$

$$EI\mathcal{K}^f a_1(0,T) = EI\mathcal{K}^f a_1(L,T) = -M, \quad (16)$$

$$U_2(0,T) = -tan\theta_o U_1(0,T), \quad (17)$$

$$(P^i + EA\triangle\epsilon)(a_1 cos\theta_o - a_2 sin\theta_o) - N + M\mathcal{K}^i cos\theta_o - K(U_1 cos\theta_o - U_2 sin\theta_o + D) + EI\mathcal{K}^f(a_{2,s} + \mathcal{K}^i a_1)cos\theta_o + EI(\mathcal{K}^f a_1)_{,s} sin\theta_o = 0 \quad at \quad S = 0. \quad (18)$$

The latter two boundary conditions (17) and (18) follow from (12) after accounting for the geometric condition $\delta U_2(0,T) = -tan\theta_o \delta U_1(0,T)$ which is required for vanishing vertical motion of the left support.

For convenience in the subsequent analysis, the following nondimensional quantities are presently introduced:

$$s = \frac{S}{L}, \quad \kappa = L\mathcal{K}^i, \quad u_1 = \frac{U_1}{L}, \quad u_2 = \frac{U_2}{L}, \quad d = \frac{D}{L},$$

$$n = \frac{NL^2}{EI}, \quad m = \frac{ML}{EI}, \quad k = \frac{KL^3}{EI}, \quad \gamma = \frac{AL^2}{I},$$

$$t = T\sqrt{\frac{EI}{\rho AL^4}}, \quad c^2 = \frac{\rho A(LC)^2}{EI}, \quad p = \frac{P^i L^2}{EI}.$$

3. Equilibrium States

The model is first used to determine all possible equilibrium states for the translating beam. The equations of equilibrium are extracted from the equations of motion (13)-(14) and the boundary conditions (15)-(18) by equating the dynamic displacement components U_1 and U_2 to zero. This procedure gives the following nonlinear boundary-value problem for solution of the (nondimensional) equilibrium centerline curvature $\kappa(s)$ and beam tension $p(s)$:

$$p' + \kappa\kappa' = 0, \qquad 0 < s < 1, \quad (19)$$

$$(p - c^2)\kappa - \kappa'' = 0, \qquad 0 < s < 1, \quad (20)$$

with the boundary conditions

$$\kappa(0) = \kappa(1) = -m, \quad (21)$$

$$p(0)cos\theta_o + \kappa'(0)sin\theta_o = n + kd. \quad (22)$$

Note that the linearized equilibrium problem, studied by Chubachi[5], follows from (19)-(22) upon using the small angle approximations $sin\theta \approx \theta$ and $cos\theta \approx 1$. The elementary linear problem admits a solution provided the speed parameter $\alpha^2 = c^2 - n$ is *not* an eigenvalue of the associated homogeneous problem ($m = 0$). The eigenvalues, $\alpha = J\pi, J = 1, 2\ldots$, give the critical speeds, $c = \sqrt{(J\pi)^2 + n}$, for divergence instability in the simply-supported, perfectly straight beams studied by Chubachi[5], Mote[8], and Simpson[9].

The existence of these eigenvalues in the linearized problem suggests the existence of multiple solutions and solution bifurcations in the complete nonlinear problem (19)-(22). Indeed, exact analysis of the nonlinear problem[10] reveals that, in general, multiple solutions exist in the *super-critical speed region* define by $c > \sqrt{\pi^2 + n}$. In reference [10], closed form expressions for these multiple solutions are derived in terms of elliptic integrals. Here, key results from [10] are briefly reviewed which are essential to the following stability analysis.

The axially moving beam equilibrium problem resembles an elastica buckling problem[6] wherein the translation speed plays the role of the buckling parameter[11]. This similarity is evident in Figure 2 which shows how θ_o, the angle of inclination of the beam centerline at the left support, depends on the translation speed. For the simplest case of vanishing bending moment ($m = 0$; see dotted curves), the equilibrium problem is homogeneous and the trivial solution $\theta_o = 0$ is always a solution. The trivial solution is the only solution in the *sub-critical speed region* defined by $c < \sqrt{\pi^2 + n}$. At the first critical speed, $c = \sqrt{\pi^2 + n}$, a pair of non-trivial solutions bifurcate from the trivial solution and lead to symmetric equilibrium shapes resembling the fundamental buckling mode of a simply supported beam[10]. Additional pairs of non-trivial solutions appear as the translation speed passes each higher-order critical speed, $c = \sqrt{(J\pi)^2 + n}$ for $J = 2, 3\ldots$, where the index J denotes the solution order. The three branches of the fundamental solution $J = 1$ in Figure 2 are presently termed the "right-branch" ($\theta_o > 0$), the "middle-branch" ($\theta_o < 0$, nearest trivial) and the "left-branch" ($\theta_o < 0$) equilibria and are central to the stability analysis of Section 4.

Multiple solutions also exist when external bending moments are applied as shown by the cases $m = .25$ (solid curves) and $m = .5$ (dashed curves) of Figure 2. In these cases, the bending moments may be interpreted as an imperfection which leads to the unfolding of all the odd-order bifurcations ($J = 1, 3\ldots$) associated with the solution for which $m = 0$. By contrast, the (symmetrically applied) bending moments have no influence on the antisymmetric

buckling modes associated with the even-order bifurcations ($J = 2, 4 \ldots$). Consequently, the even-order bifurcations remain folded. Note that for $m \neq 0$, the speed first required to produce multiple solutions is always *greater than* the fundamental critical speed and that it increases with increasing bending moment. This speed and the second critical speed play key roles in the stability of the equilibria.

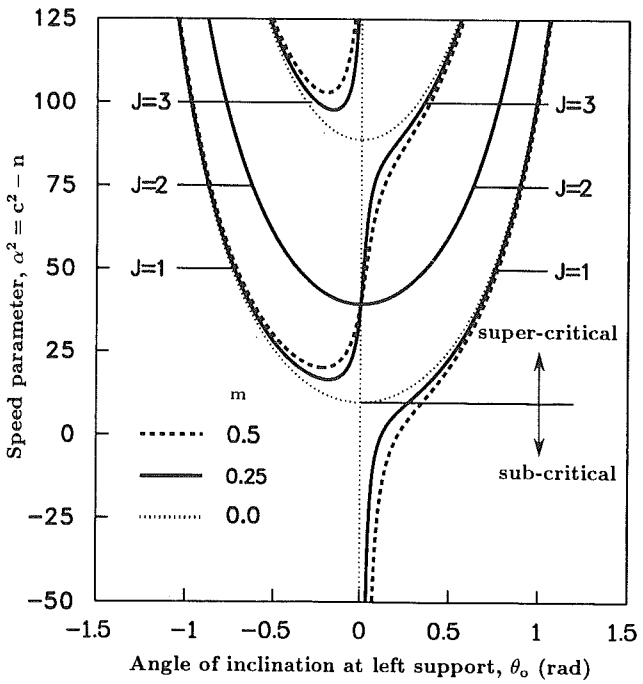

Figure 2: Multiple solutions, bifurcations and unfoldings in the equilibrium problem[10] . Result shown in the $\alpha^2 - \theta_o$ plane for the cases $m = .5$, .25 and 0. In all cases $n = 100$ and $k = 0$. The index J denotes the order of the solution.

4. Linear Vibration and Stability Analysis

It is important to emphasize that all previous stability analyses of an axially moving beam have focused exclusively on the stability of the *trivial* equilibrium. *The existence and possible stability of the non-trivial equilibria described above have been overlooked.*

To investigate the stability of all equilibria, the nonlinear equations of motion are linearized about an arbitrary equilibrium having curvature $\kappa(s)$ and tension $p(s)$. The linearized, homogeneous (nondimensional) equations governing free, planar response are:

tangential component, u_1

$$[(\gamma+p-c^2)(u_{1,s}-\kappa u_2)]_{,s}+[\kappa(c^2-p)][u_{2,s}+\kappa u_1]+\kappa[u_{2,s}+\kappa u_1]_{,ss} = u_{1,tt} + 2c[u_{1,s} - \kappa u_2]_{,t}, \quad (23)$$

normal component, u_2

$$[\kappa(\gamma+p-c^2)][u_{1,s}-\kappa u_2]+[(p-c^2)(u_{2,s}+\kappa u_1)]_{,s}-[u_{2,s}+\kappa u_1]_{,sss} = u_{2,tt} + 2c[u_{2,s} + \kappa u_1]_{,t}. \quad (24)$$

Assuming that the left support now remains stationary *after* the beam attains its equilibrium, the boundary conditions become:

$$u_1 = u_2 = 0, \;\; u_{2,ss} + \kappa u_{1,s} = 0, \;\; at \;\; s = 0, 1. \quad (25)$$

It should be noted that the linear equation of transverse motion for a perfectly straight translating beam[5,8,9] is obtained from (24) as the special case $\kappa(s) = 0$ and $p(s) = n$.

Motion about a specific, non-trivial equilibrium is examined after first evaluating the elliptic integral representations of the equilibrium curvature $\kappa(s)$ and tension $p(s)$[10]. These functions appear as (nonconstant) coefficients in (23) and (24). Due to the general complexity of these equations, exact solutions cannot be determined by known analytical methods. Here, approximate solutions will be determined following discretization using the Galerkin method.

Consider the R-term admissible series representations for u_1 and u_2 of the form:

$$u_i(s,t) = \sum_{j=1}^{R} \phi_{ij}(t)\Theta_j(s), \;\; i = 1, 2, \quad (26)$$

where $\Theta_j(s) = \sqrt{2}sin(j\pi s)$. Substitution of (26) into (23) and (24), and application of the Galerkin method, provides a set of $2R$ coupled, ordinary differential equations for solution of the generalized coordinates $\vec{\phi}^T(t) = [\phi_{11}(t), \;\; \phi_{12}(t), ..., \phi_{2R}(t)]$:

$$\mathbf{M}\ddot{\vec{\phi}} + \mathbf{G}\dot{\vec{\phi}} + \mathbf{K}\vec{\phi} = \vec{0}. \quad (27)$$

The elements of these matrices, which are given in the Appendix, are evaluated by numerical quadrature.

The natural frequencies and mode shapes for the translating beam are obtained through the eigensolutions of the discretized model (27). In the present formulation, the natural frequencies of the translating beam are given by the imaginary parts of the eigenvalues, $\omega_l, l = 1, 2 \ldots 2R$, and the mode shapes are obtained from the eigenvectors through (26). A divergence instability for mode l is identified when $Im(w_l) \rightarrow 0$. In calculations, the series size $R = 10$ was used and the eigensolutions described below have fully converged.

As a primary example, consider the stability of a translating beam subjected to the slight bending moment $m = .25$. Figure 3 shows the fundamental natural frequencies of vibration as functions of translation speed in both the sub-critical and super-critical speed regions. In the super-critical speed region, three curves are shown which depict separately the fundamental frequencies of vibration about the right-branch, middle-branch and left-

branch equilibria shown in Figure 2 for the (fundamental) equilibrium solution $J = 1$. The fundamental frequency of vibration about the trivial equilibrium is also shown to facilitate a comparison with the model of a perfectly straight beam[5,8,9]. In this latter case, the dotted curve indicates that the fundamental frequency decreases with translation speed and vanishes at the lowest critical speed $\sqrt{\pi^2 + n}$. Thus, as is well known from previous studies, *the stability of a perfectly straight beam is limited to the sub-critical speed region. Stability, however, is never lost when any degree of initial beam curvature is introduced.* The solid curve in Figure 3, which depicts the fundamental frequency of vibration about the right-branch equilibrium, clearly shows that this equilibrium never loses stability over the indicated speed range. While the fundamental frequency decreases in the sub-critical speed region, it rapidly *increases* in the neighborhood of the critical speed. This effect derives mainly from the stiffening of the beam as its curvature markedly increases near the critical speed; see region of rapid growth of θ_o for the right-branch equilibrium ($J = 1$) of Figure 2. Likewise, the left-branch equilibrium remains stable in the super-critical speed region as seen by the dashed curve of Figure 3. The middle-branch equilibrium, however, does experience a divergence instability at a speed above the former first "critical speed"; see dash-dot curve of Figure 3.

In Figure 3, the fundamental frequencies for the two stable equilibria (right and left-branch) are nearly identical for large super-critical speeds. This results from the fact that their respective equilibrium shapes become nearly mirror images at large translation speeds[10]; observe also the magnitudes of θ_o for the right and left-branch equilibria in Figure 2. In Figure 3, also note that the fundamental frequency associated with the trivial equilibrium provides a lower bound to that associated with the right-branch equilibrium for sub-critical speeds. This behavior can again be anticipated from Figure 2 which shows that the trivial equilibrium itself is a reasonable approximation to the right-branch equilibrium in the sub-critical speed region. Finally, it should be noted that the fundamental eigenvalues computed for the higher-order equilibrium solutions depicted in Figure 2 for $J = 2, 3 \ldots$ indicate that they are unstable.

The natural frequencies of the second and higher-order vibration modes follow trends similar to that of the fundamental mode as illustrated by the results in Figure 4. The first four natural frequencies for vibration about the right, middle, and left-branch equilibria are plotted versus translation speed together with those associated with the trivial equilibrium[5,8,9]. An important point to note from this plot is that the fundamental frequency associated with the middle-branch equilibrium vanishes precisely at the *second* critical speed associated with the trivial equilibrium. Recall from Figure 2 that the bifurcation occurring at the second critical speed $c = \sqrt{(2\pi)^2 + n}$ is unaffected by the (symmetrically applied) bending moments and remains folded. Indeed, at the second critical speed, the middle-branch equilibrium *is* the trivial equilibrium. Beyond this speed, the middle-branch equilibrium solution

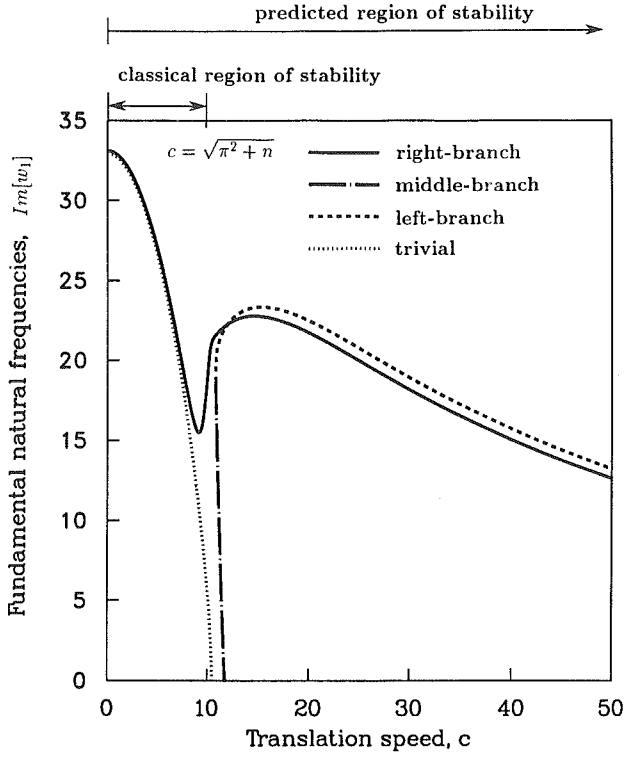

Figure 3: Stability of an axially moving beam with slight initial curvature. The fundamental frequencies of vibration are plotted versus translation speed for vibration about the right, middle and left-branch equilibria ($J = 1$) of Figure 2. In this example, $m = 0.25$, $n = 100$, and $k = 0$. Dotted curve represents fundamental frequency of vibration about trivial equilibrium.

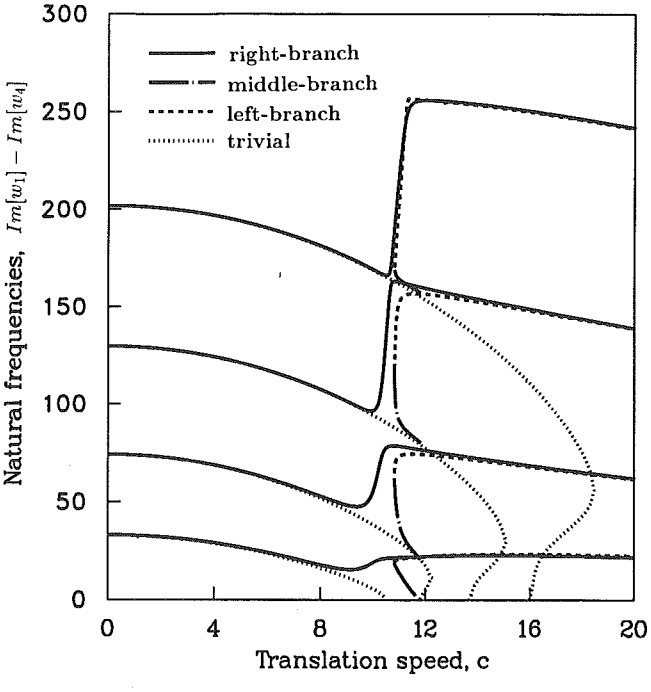

Figure 4: Higher order natural frequencies. Plot shows first four natural frequencies of vibration about the right, middle and left-branch equilibria ($J = 1$) of Figure 2. In this example, $m = 0.25$, $n = 100$, and $k = 0$. Dotted curves represent natural frequencies for vibration about trivial equilibrium.

bifurcates (see Figure 2) and the present eigensolution, based on the fundamental ($J = 1$) equilibria, is not continued for the unstable portion of the middle-branch.

The stable fundamental modes for vibration about the right, middle and left-branch equilibria are illustrated in Figure 5 for the case where the translation speed is 10% greater than the first critical speed. The dotted curves depict the super-critical equilibrium shapes and the solid curves depict the beam at various times as it oscillates at its natural frequency over one period. As with all axially moving material (gyroscopic) systems, the free response has non-uniform phase due to the existence of complex eigenfunctions[1,9]. Note that, even at this modest super-critical translation speed, the right and left-branch equilibria are already nearly mirror images.

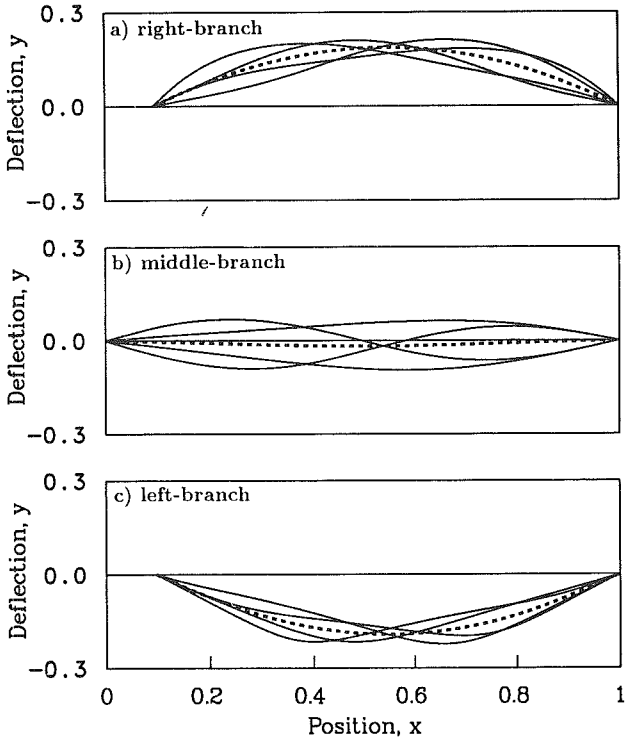

Figure 5: Fundamental mode shapes at super-critical speed $c/\sqrt{\pi^2+n} = 1.10$. Results shown for vibration about a) right, b) middle and c) left-branch equilibria ($J = 1$) in Figure 2. Solid curves depict beam profile at times $t = 0$, $.25\tau$, $.75\tau$, and τ, where τ is the fundamental period of oscillation. Dashed curves depict equilibrium beam profiles. In all cases $m = 0.25$, $n = 100$, and $k = 0$.

5. Summary and Conclusions

A dynamical model for an axially moving beam is presented which accounts for the initial beam curvature generated by supporting wheels and pulleys. The model considers geometrically nonlinear beam deflections and is therefore capable of describing the large response expected at critical and super-critical translation speeds.

Analysis of the equations of equilibrium[10] reveals that the beam undergoes large static deflections near the first critical speed predicted by previous studies[5,8,9] of geometrically perfect beams. Slightly above this speed, three equilibrium states exist which are referred to here as the right-branch, middle-branch and left-branch equilibria. For the idealized case of no initial curvature, these multiple equilibrium states appear as a folded bifurcation of the trivial equilibrium at the first critical speed. When the beam possesses any initial (symmetric) curvature, the bifurcation unfolds and a larger translation speed is required to generate multiple equilibria.

The equations of motion are linearized about the equilibria and their stability is determined from the eigensolutions of a discretized model. For the idealized case of no initial curvature, the trivial equilibrium experiences a divergence instability at the first critical speed[5,8,9]. The beam then buckles and forms either the right or left-branch equilibria which are both stable in the super-critical speed region. When the beam possesses *any* degree of initial curvature, however, no divergence instability exists at the first "critical speed." In this case, the equilibrium state in the sub-critical speed region is a continuous extension of the right-branch equilibrium and the beam never looses stability. The left-branch equilibrium also remains stable after it appears in the super-critical speed region.

In summary, the results herein indicate that critical speed behavior in axially moving material problems represents an idealized phenomenon which does not occur when imperfections, such as initial curvature, are present.

Acknowledgments

The authors gratefully acknowledge the support of the University of Michigan Office of the Vice President for Research and the partial support of the U. S. Office of Naval Research.

References

[1] Mote, C. D., Jr., 1972, "Dynamic Stability of Axially Moving Materials," *Shock and Vibration Digest*, vol. 10, no. 4, pp. 2-11.

[2] Wickert, J. A. and Mote, C. D., Jr., 1988, "Current Research on the Vibration and Stability of Axially Moving Materials," *Shock and Vibration Digest*, vol. 20, no. 5, pp. 3-13.

[3] Perkins, N. C. and Mote, C. D., Jr., 1987, "Three-Dimensional Vibration of Traveling Elastic Cables," *Journal of Sound and Vibration*, vol. 114, no. 2, pp. 325-340.

[4] Perkins, N. C., 1990, "Asymptotic Analysis of a Translating Cable Arch," *Journal of Sound and Vibration*, in press.

[5] Chubachi, T., 1957, "Lateral Vibration of Axially Moving Wire or Belt Form Materials," *Bulletin of JSME*, vol. 23, no. 127, pp. 205-210.

[6] Love, A. E. H., 1944, *A Treatise on the Mathematical*

Theory of Elasticity, fourth edition, Dover, New York, Ch. 21.

[7] Benjamin, T. B., 1961, "Dynamics of a System of Articulated Pipes Conveying Fluid –Part I: Theory, and Part II: Experiment," *Proceedings of the Royal Society*, series A, vol. 261, pp. 457-499.

[8] Mote, C. D., Jr., 1965, "A Study of Bandsaw Vibrations," *Journal of the Franklin Institute*, vol. 279, no. 6, pp. 430-444.

[9] Simpson, A., 1973, "Transverse Modes and Frequencies of Beams Translating Between Fixed End Supports," *Journal of Mechanical Engineering Science*, vol. 15, no. 3, pp. 159-164.

[10] Hwang, S.-J. and Perkins, N. C., 1990, "Nonlinear Equilibrium Analysis of Axially Moving Materials," submitted to the *CSME Mechanical Engineering Forum*, Toronto, Canada, June 1990.

[11] Thompson, J. M. T., and Lunn, T. S., 1981, "Static Elastica Formulations of a Pipe Conveying Fluid," *Journal of Sound and Vibration*, vol. 77, no. 1, pp. 127-132.

Appendix

The discretized equations of motion are given by

$$\mathbf{M}\begin{bmatrix} \ddot{\phi}_{11} \\ \ddot{\phi}_{12} \\ \cdot \\ \cdot \\ \ddot{\phi}_{2R} \end{bmatrix} + \mathbf{G}\begin{bmatrix} \dot{\phi}_{11} \\ \dot{\phi}_{12} \\ \cdot \\ \cdot \\ \dot{\phi}_{2R} \end{bmatrix} + \mathbf{K}\begin{bmatrix} \phi_{11} \\ \phi_{12} \\ \cdot \\ \cdot \\ \phi_{2R} \end{bmatrix} = \vec{0},$$

where the $2R \times 2R$ coefficient matrices are

$$\mathbf{M} = \begin{bmatrix} \mathbf{M11} & 0 \\ 0 & \mathbf{M22} \end{bmatrix}, \mathbf{G} = \begin{bmatrix} \mathbf{G11} & \mathbf{G12} \\ \mathbf{G21} & \mathbf{G22} \end{bmatrix},$$

$$\mathbf{K} = \begin{bmatrix} \mathbf{K11} & \mathbf{K12} \\ \mathbf{K21} & \mathbf{K22} \end{bmatrix}.$$

Letting <a, b>=$\int_0^1 a(s)b(s)ds$, the sub-matrices $\mathbf{M}_{11}, \ldots, \mathbf{K}_{22}$ are

$$\mathbf{M11}(i,j) = \mathbf{M22}(i,j) = < \theta_i, \theta_j > = \delta_{ij} \quad \text{(Kronecker's delta)},$$

$$\mathbf{G11}(i,j) = \mathbf{G22}(i,j) = 2c < \theta_i, \theta_j' >,$$
$$\mathbf{G12}(i,j) = -\mathbf{G21}(j,i) = -2c < \theta_i, \kappa\theta_j >,$$

$$\mathbf{K11}(i,j) = < (\kappa\theta_i)', (\kappa\theta_j)' > + < \theta_i, \kappa^2(p-c^2)\theta_j > + < \theta_i', (p+\gamma-c^2)\theta_j' >,$$
$$\mathbf{K22}(i,j) = < \theta_i'', \theta_j'' > + < \theta_i', (p-c^2)\theta_j' > + < \theta_i, \kappa^2(p+\gamma-c^2)\theta_j >,$$
$$\mathbf{K12}(i,j) = \mathbf{K21}(j,i) = < (\kappa\theta_i)', \theta_j'' > + < \theta_i, \kappa(p-c^2)\theta_j > + < \theta_i', -\kappa(p+\gamma-c^2)\theta_j >,$$

where $i, j = 1, 2, \ldots, R$ and $\theta_j(s) = \sqrt{2}sin(j\pi s)$. The equilibrium curvature $\kappa(s)$ and tension $p(s)$ are obtained from solution of the equilibrium problem[10].